Imaging Studies of the Photodissociation of NH_3^+ and ND_3^+ Cations†

Alexander D. Webb, N. Hendrik Nahler,‡ and Michael N. R. Ashfold*

School of Chemistry, University of Bristol, Bristol, BS8 1TS, U.K.

Received: October 7, 2008; Revised Manuscript Received: January 8, 2009

Velocity map ion imaging methods have been used to study the photofragmentation dynamics of state-selected NH_3^+ and ND_3^+ cations. The cations were prepared in selected υ_2^+ bending vibrational levels of the ground ($\tilde{X}^2A''$) electronic state by two-photon resonant, three-photon ionization of $NH_3(ND_3)$, via several different υ_2' levels of the $\tilde{B}$ and $\tilde{C}'$ Rydberg states. Subsequent excitation to the $\tilde{A}^2E$ state by absorption of a 207.6 nm photon resulted in N−H(D) bond fission and $NH_2^+(ND_2^+)$ fragment ion formation. These fragments exhibit isotropic recoil velocity distributions, which peak at low kinetic energy but extend to the maximum allowed by energy conservation. Such findings accord with conclusions from earlier electron induced photoionization and photoelectron-photoion coincidence studies of NH_3 at similar total energies (defined relative to the ground-state neutral) and, as previously, can be rationalized in terms of excitation to the Jahn−Teller distorted $\tilde{A}$ state, rapid radiationless transfer via one or more conical intersections linking the $\tilde{A}$ and $\tilde{X}$ state potential energy surfaces (PESs) and subsequent unimolecular decay on the latter PES. Weak NH_2^+ and NH^+ fragment ion signals are also observed when exciting with the ionization laser only; imaging these fragment ions provides some insights into their likely formation mechanisms.

1. Introduction

Ion imaging methods[1] are offering new opportunities for studying the photofragmentation dynamics of state-selected molecular cations at levels of product state resolution that begin to approach those found in (the far more numerous) photodissociation studies involving neutral molecules. Examples of cations investigated in this way include DCl^+,[2] Br_2^+,[3] $BrCl^+$,[4−6] triatomic cations like OCS^+ [7] and H_2S^+,[8,9] and a limited number of larger species, e.g., $C_2H_4^+$ [10,11] and CH_3CHO^+.[12] This paper describes the application of contemporary ion imaging methods to studies of the photofragmentation dynamics of the ammonia cation.

As with other cations, most previous studies of the fragmentation dynamics of NH_3^+ have involved excitation from the ground-state neutral molecule and centered on the use of photoelectron spectroscopy[13,14] and related coincidence methods. The ground ($\tilde{X}^2A_2''$) and first excited ($\tilde{A}^2E$) states of the ion have been most studied. The photoelectron band associated with the former, which arises as a result of ionization out of the $3a_1$ highest occupied molecular orbital, shows a long progression in the umbrella vibrational mode (ν_2^+), reflecting the planar ← pyramidal change in equilibrium geometry that accompanies loss of a $3a_1$ electron. A second (weaker) progression has been discerned also and assigned to a ν_2^+ progression built on one quantum of ν_4^+ (the degenerate in-plane bending mode). Vibronic coupling to the $\tilde{A}^2E$ state has been advanced to explain the strength of this latter progression.[14,15] Infrared absorption studies have confirmed the planar (D_{3h}) equilibrium structure of the $\tilde{X}^2A_2''$ state of NH_3^+.[16,17] The $\tilde{A}^2E$ photoelectron band, arising as a result of ionization from the 1e orbital, shows an onset at ∼14.725 eV, maxima at ∼15.8 and ∼16.8 eV, and diffuse, irregular vibronic structure,[13,14] the detailed assignment of which represents an ongoing challenge.

An early search for $NH_3^+(\tilde{A}-\tilde{X})$ fluorescence was unsuccessful. Possible explanations advanced[18] to account for the nonobservation of fluorescence included lengthening of the radiative lifetime through resonant mixing of the $\tilde{A}^2E$ levels with high rovibrational levels of the $\tilde{X}$ state and/or the operation of one or more fast nonradiative decay processes from the $\tilde{A}$ state. Many theoretical studies[15,19−23] have since appeared that support the latter view. Haller et al.[19] showed that the gross contour of the $\tilde{A}^2E$ photoelectron band is determined by the strong Jahn−Teller (JT) activity of the asymmetric stretching and bending modes (ν_3 and ν_4). The overall width and shape of the $\tilde{A}^2E$ band were qualitatively reproduced by this two-mode model, but subsequent inclusion of a further (ν_4-mediated) pseudo-JT coupling between the $\tilde{A}$ and $\tilde{X}$ states provides a much better match to the observed band contour and the diffuse structures.[15] The significant effect of the $\tilde{A}-\tilde{X}$ pseudo-JT coupling is attributable to interaction between the (lower component of the) adiabatic $\tilde{A}^2E$ state potential energy surface (PES) and the ground-state PES. Time-dependent quantum wavepacket calculations on these coupled PESs suggest substantial (though not total) decay of $\tilde{A}$ state population via a conical intersection (CI) with the $\tilde{X}$ state PES within ∼30 fs.

Locht et al.[24] investigated $NH_2^+(ND_2^+)$ and $NH^+(ND^+)$ fragment formation following electron-induced dissociative ionization of NH_3^+ and ND_3^+ at incident electron energies <50 eV. Kinetic energy distributions for both sets of products were measured following excitation in the energy range spanned by the $\tilde{A}^2E$ photoelectron band; those for the $NH_2^+(ND_2^+)$ fragments showed some structure and were rationalized in terms of predissociation mediated by a CI linking the $\tilde{A}$ and $\tilde{X}$ states, while those for the $NH^+(ND^+)$ fragments were broad and structureless. The photofragmentation of $\tilde{A}$ state NH_3^+ cations has also been investigated by photoelectron-photoion coincidence (PEPICO) methods.[25,26] An early (room temperature) study[25] identified an onset for NH_2^+ fragment ion formation at

† Part of the George C. Schatz Festschrift.

* Corresponding author. Tel: (117)-9288312/3. Fax: (117)-9250612. E-mail: mike.ashfold@bris.ac.uk.

‡ Current address: Department of Chemistry, University Science Laboratories, South Road, Durham, DH1 3LE, U.K.

10.1021/jp808854d CCC: $40.75
Published on Web 02/13/2009

photon energies of ~15.5 eV and determined that the quantum yield for NH_2^+ formation by N−H bond fission was unity at photon energies >15.9 eV. The total kinetic energy release (TKER) spectrum of the H + NH_2^+ products was found to peak at low KE (implying that most of the available energy was retained as internal excitation of the NH_2^+ fragment) and to have a form that matched well with predictions derived by application of phase-space theory and the assumption that population was distributed statistically among the energetically accessible product states, subject only to certain angular momentum constraints. More recent high-resolution PEPICO studies[26] yielded a more precise threshold energy for forming NH_2^+ fragment ions: 15.765 ± 0.001 eV (measured relative to the zero-point level of ground-state NH_3). This, in turn, gave a measure of the N−H bond strength in NH_3^+, $D_0(H_2N^+-H)$ = 5.579 ± 0.001 eV, given a value of 10.1864 ± 0.0001 eV (82 159 ± 1 cm^{-1}) for the ionization potential (IP) of NH_3.[27] Recent pulsed field ionization (PFI) zero-kinetic-energy (ZEKE) photoelectron spectroscopy studies of the NH_2 radical returned IP(NH_2) = 90083.8 ± 1 cm^{-1},[28] which, when combined with $D_0(H_2N-H) = 37115 \pm 20$ cm^{-1},[29] yields a mutually consistent value for $D_0(H_2N^+-H)$.

Numerous resonance enhanced multiphoton excitation and ionization (REMPI) studies of NH_3 (and ND_3) have been reported.[30] Two studies are of particular relevance to the present investigations. Colson and co-workers[31] examined the mass and photoelectron spectra obtained following MPI of both isotopologues at wavelengths chosen to achieve resonance enhancement by selected vibrational levels of the $\tilde{B}$, $\tilde{C}'$ and $\tilde{D}$ Rydberg states lying at the energy of three absorbed photons. The measured mass spectra clearly show formation of fragment ions, but only at energies above the threshold for accessing the $\tilde{A}$ state of the parent ion. Different resonance-enhancing levels were found to show characteristically different REMPI photoelectron KE distributions. Excitation via different bending (v_2') levels of the $\tilde{C}'$ state revealed a strong propensity for $\Delta v = (v_2^+ - v_2') = 0$ transitions in the ionization step, and thus for forming state-selected NH_3^+(ND_3^+) cations. The photoelectron spectra obtained following excitation via the $\tilde{B}$ and $\tilde{D}$ states tended to be richer, revealing evidence for competing autoionization processes and, in the case of $\tilde{D}$ state, of vibronic mixing between levels of the $\tilde{D}$ and $\tilde{B}$ states. Zare's group[32] later reported photoelectron KE measurements following two-photon resonant, three-photon ionization (i.e. 2 + 1 REMPI) via selected levels of the $\tilde{B}$ and $\tilde{C}'$ states of NH_3, which revealed a high propensity for $\Delta v = 0$ transitions in the ionization step (with >80% retention of the v_2 quantum number upon ionization via $\tilde{C}'$ state levels with $0 \le v_2 \le 6$ and >70% conservation in case of ionization via $\tilde{B}$ state levels with $3 \le v_2 \le 10$).

Here we employ velocity map ion imaging methods[33] to perform the first direct photofragmentation studies of vibrationally state-selected NH_3^+(ND_3^+) cations. The parent cations are formed by 2 + 1 REMPI via selected levels of the $\tilde{B}$ and $\tilde{C}'$ states and then fragmented by absorbing one (or more) further photons. Image analysis yields the fragment cation velocities and thus the product TKER distributions, which yield insights into the product branching ratios, the dissociation dynamics, and any contributions from unintended, competing nonresonant multiphoton dissociative ionization processes.

2. Experimental Section

The velocity map imaging apparatus[34] and its use in studies of the photodissociation of state-selected molecular cations[2,8] have both been described previously. NH_3 and ND_3 were obtained commercially (>99.5% and >99% stated purity, respectively) and subsequently diluted to ~10% mixtures in Ar in separate glass bulbs (total pressure ~760 Torr). A skimmed molecular beam of the mixture of interest was intersected at right angles by two counter-propagating laser beams. For all measurements, the electric vectors ($\boldsymbol{\varepsilon}$) of both lasers were set perpendicular to the time-of-flight (TOF) axis and thus parallel to the front face of the microchannel plates that form part of the ion detection system. All measured images should thus be cylindrically symmetric about the polarization (vertical) axis. Analysis of each image involved reconstruction of the three-dimensional velocity distribution from the recorded two-dimensional projection and a radial integration as described previously.[34]

Parent cations were formed by REMPI, using the output of a Nd:YAG pumped dye laser (Spectra-Physics GCR-170 plus PDL-2) and subsequent frequency doubling to yield a range of UV excitation wavelengths λ_1 (with pulse energies in the range 0.1−1 mJ), which were focused into the interaction region (20 cm f.l. lens). Most experiments employed two photon excitation to levels of the $\tilde{C}'$ state (with $v_2' = 0-4$, 6, and 7 in the case of NH_3 and $v_2' = 3-6$ and 9 for ND_3). Excitations via various combination levels (e.g. the $\tilde{C}',1^1 2^3$ level of NH_3) were attempted also, but the eventual fragment ion signals were prohibitively small. NH_3^+ and ND_3^+ cations were also formed by two-photon resonant MPI via selected levels of the $\tilde{B}^1E''$ state (with $v_2' = 0-2$ and 6 (NH_3) and $v_2' = 3-6$, 8, 11, and 12 (ND_3)). For both resonance-enhancing states, the excitation wavelength was typically set to excite one (or more) Q branch transitions, but several $\Delta J \neq 0$ branch lines were excited also. None of the measured images showed any discernible sensitivity to the choice of rotational quantum number or branch.

As described below, the REMPI laser alone produced a weak fragment ion signal, a process that we term "one-color" photodissociation. Additional fragmentation could be induced by introducing a second laser pulse, of wavelength λ_2, delayed by δt = 5−150 ns relative to the REMPI laser pulse. The temporal separation was defined and controlled by a digital delay generator (BNC Model 555) and measured using a fast photodiode linked to an oscilloscope (Tektronix TDS 3012). The longer delays were explored in an attempt to reduce the effect of space-charge, as demonstrated in studies of OCS^+ photolysis.[7] The "two-color" fragment ion yields were also low and required the use of long integration times (images were typically taken for $\ge 2 \times 10^4$ laser shots and in most cases images repeated three or four times to ensure consistency in the data). All cation photolyses reported here used a Sirah Cobra Stretch dye laser (pumped by a Spectra-Physics GCR 250 Nd:YAG laser), operating at a wavelength of 415.24 nm, with subsequent frequency doubling (BBO-A) crystal to yield λ_2 = 207.6 nm radiation. The choice of this particular wavelength was dictated by the Woods anomaly of the diffraction grating;[35] the resulting laser pulses (energy ~2 mJ) were focused (20 cm f.l. lens) into the interaction region.

3. Results and Discussion

The following describes, in turn, analysis of images of NH_2^+(ND_2^+) fragments resulting from, first, one-color ionization and dissociation of NH_3(ND_3) molecules and, second, two-color experiments in which state-selected NH_3^+(ND_3^+) ions are photolyzed by a second laser, before a brief description of imaging studies of NH^+(ND^+) fragment ions.

3.1. One-Color Studies of NH_2^+ Product Formation. TOF mass spectra of the ions formed by REMPI of NH_3, recorded

at many different excitation wavelengths, serve to illustrate the striking propensity for forming parent ions. Under the experimental conditions employed in the present work, the fragment ion yield was less ~0.2% (relative to the parent ion signal) when exciting through the $v_2' = 0$ level of the $\tilde{B}$ or $\tilde{C}'$ states. This fraction increased as the REMPI wavelength was decreased, but for both intermediate states, it was still <5% when $v_2' = 6$.

Figure 1 displays raw images of the NH_2^+ fragment ions recorded following excitation of NH_3 at (a) $\lambda_1 = 296.3$ nm ($\tilde{\nu} = 33\,753$ cm^{-1}) and (b) $\lambda_1 = 287.9$ nm (34 737 cm^{-1})—chosen to be two-photon resonant with the Q branches of, respectively, the $\tilde{C}'-\tilde{X}$ 2_0^4 and 2_0^6 transitions—along with the TKER distributions derived there from. Both peak near zero and neither shows any obvious fine structure.

One can envisage (at least) two routes by which such NH_2^+ fragment ions might arise. One, inspired by a previous explanation for the photon energy dependence of the fragment ion yield accompanying REMPI of NH_3 and ND_3,[31] involves absorption of four photons of frequency ν_1 and subsequent dissociative ionization, i.e.

$$NH_3(\tilde{X}^1A_1) + 4h\nu_1 \rightarrow NH_2^+ + H + e^- \quad (1)$$

The vertical arrows superposed on Figure 1a,b indicate the maximum TKERs compatible with such a mechanism. The earlier REMPI photoelectron studies of NH_3[31] demonstrated a strong propensity for $\Delta v = (v_2^+ - v_2') = 0$ ionizing transitions from the $\tilde{B}$ and $\tilde{C}'$ states. Thus, an alternative route to forming NH_2^+ fragments under the present experimental conditions would involve a sequence in which NH_3 is ionized, state-selectively, by 2 + 1 REMPI, and the resulting $NH_3^+(\tilde{X})$ cations are then photolyzed by further absorption of one (or more) photons from within the same laser pulse, e.g.

$$NH_3(\tilde{X}^1A_1) + 2h\nu_1 \rightarrow NH_3(\tilde{C}', v_2') \quad (2)$$

$$NH_3(\tilde{C}', v_2') + h\nu_1 \rightarrow NH_3^+(\tilde{X}, v_2^+) + e^- \quad (3)$$

$$NH_3^+(\tilde{X}, v_2^+) + nh\nu_2 \rightarrow NH_2^+ + H \quad (4)$$

with $\nu_2 = \nu_1$ in the case of one-color dissociation induced by the REMPI laser and $n \geq 2$.

The low fragment ion yields in the present one-color experiments can be understood by recognizing that (i) most parent molecules undergo 2 + 1 REMPI and form NH_3^+ ions rather than the four-photon dissociative ionization process 1, but (ii) one-photon absorption by, for example, $NH_3^+(\tilde{X}, v_2^+ = 6)$ cations provide insufficient energy to exceed $D_0(H_2N^+-H)$, and (iii) the cross-section for $NH_3^+(\tilde{A}-\tilde{X})$ two-photon absorption is small.[31] The maximum possible TKER of $H + NH_2^+(\tilde{X})$ fragments arising via sequence 2−4 with $n = 2$ in process 4 is >30 000 cm^{-1}, but examination of Figure 1 provides no indication of any such fast fragments. Thus, the present findings tend to support the previous view[31] that the NH_2^+ fragment ions formed in the one-color multiphoton excitation of NH_3 arise via process 1. Given such an interpretation, analysis of the measured images indicates that <5% of the available energy (i.e., $4h\nu_1 - 15.765$ eV) is released in the form of fragment KE. Such energy disposal is consistent with earlier findings [24,31] and with the "statistical" energy partitioning that appears to be typical of such three-body dissociative ionization processes.

We recognize a number of possible ambiguities in interpreting the results of such one-color experiments. The NH_2^+ ion has a low-lying excited state, the $\tilde{a}^1A_1$ state, which lies ~1.3 eV above the ground $\tilde{X}^3B_1$ state. The maximum possible TKER of any H + NH_2^+(a) fragments formed via process 1 is indicated by a dashed arrow in Figure 1b; the photon energy used to obtain the data shown in Figure 1a is insufficient to produce NH_2^+(a) products via process 1. Clearly, this electronically excited-state could contribute to the overall product yield in Figure 1b and at shorter excitation wavelengths. Further, neither mechanism 1 nor 2−4 can be definitely confirmed at present, as two-photon-induced dissociation of the parent ion could, in principle, yield a highly inverted population distribution in the NH_2^+ products. The two-color experiments reported below were designed, in part, to resolve between such alternative interpretations.

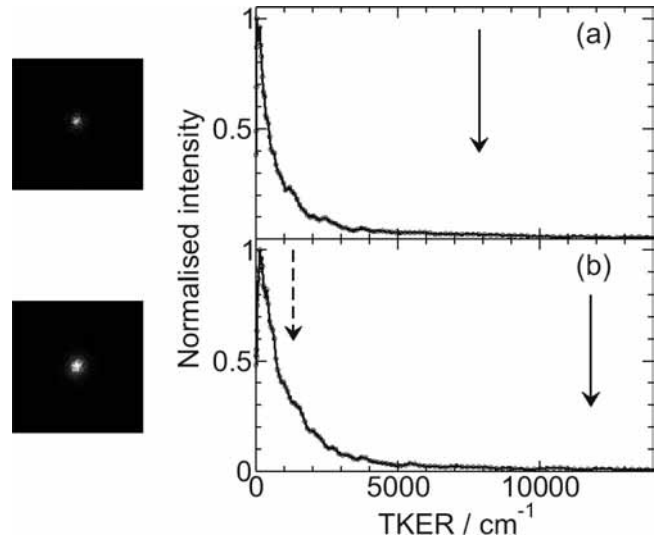

Figure 1. NH_2^+ fragment ion images and the associated H + NH_2^+ product TKER distributions resulting from one-color multiphoton excitation of NH_3 at (a) $\lambda_1 = 296.3$ nm ($\tilde{\nu}_1 = 33\,753$ cm^{-1}) and (b) $\lambda_1 = 287.9$ nm ($\tilde{\nu}_1 = 34\,737$ cm^{-1}). The solid vertical arrow superimposed above each distribution indicates the maximum possible TKER of the H + NH_2^+ fragments arising via process 1, while the dashed arrow in panel b indicates the maximum TKER of such products in the case that the NH_2 fragment is formed in its $\tilde{a}^1A_1$ state.

3.2. Two-Color Studies of NH_2^+ and ND_2^+ Product formation. Given $D_0(H_2N^+-H) = 5.579 \pm 0.001$ eV,[26] the long wavelength threshold for forming NH_2^+ fragments from $NH_3^+(\tilde{X}, v^+ = 0)$ parent ions is $\lambda_2 \leq 222$ nm. The one-color TOF mass spectrum obtained when such short wavelength radiation is focused into the interaction region shows peaks indicating formation of NH_3^+ and, with much lower probability, NH_2^+ and NH^+ ions, even when the REMPI laser radiation required to induce NH_3^+ parent ion formation via processes 2 and 3 is blocked. This observation can be understood as follows: The $\tilde{A}^1A_2'' \leftarrow \tilde{X}^1A_1$ absorption cross-section of neutral NH_3 is nonzero at $\lambda < 220$ nm,[14] and thus provides resonance enhancement to the two-photon ionization of NH_3 at such wavelengths. The $NH_3(\tilde{A})$ state possesses substantial valence character and is heavily predissociated.[29,36] As a result, the NH_3^+ ions formed by 1 + 1 REMPI via this state are distributed over a range of vibrational states.[31] Absorption of an additional photon by these parent ions results in the observed fragment ions.

High REMPI laser intensities result in large NH_3^+ yields and contribute unwanted NH_2^+ fragment ion signal. Space charge effects (due to the large parent ion yield) can also blur and distort the fragment ion images. The probability of parent ion photolysis by the second laser pulse should scale with its intensity, but as discussed above, the dissociation laser can also act as an unwanted one-color source of fragment ions. The recording of two-color images was thus a delicate balancing act, wherein the REMPI and dissociation laser intensities, their wavelengths,

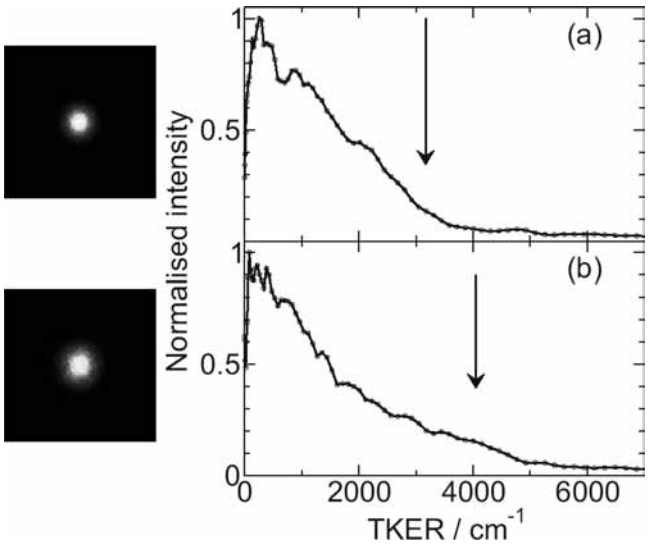

Figure 2. NH_2^+ fragment ion images and the associated TKER distributions resulting from 2 + 1 REMPI of NH_3 via (a) the $\tilde{C}'$ ($v_2' = 0$) and (b) the $\tilde{C}'$ ($v_2' = 1$) levels with subsequent photolysis of the resulting parent cations at $\lambda_2 = 207.6$ nm after $\delta t \sim 20$ ns. The arrow in each panel indicates the maximum TKER of the H + $NH_2^+(\tilde{X})$ products resulting from one photon dissociation of parent cations with $v_2^+ = v_2'$.

and their relative timings all require careful optimization to ensure that neither laser alone made a significant contribution to the two-color images reported here.

Figure 2 shows images and speed distributions of NH_2^+ fragments resulting from 207.6 nm photolysis of $NH_3^+(\tilde{X})$ cations prepared by 2 + 1 REMPI of NH_3 via, respectively, the $v_2' = 0$ (a) and $v_2' = 1$ (b) levels of the $\tilde{C}'$ state. The images are small and display no discernible recoil anisotropy. In both cases, the TKER distributions of the H + NH_2^+ fragments extend to the maximum allowed by energy conservation (marked by the vertical arrows in Figure 2 and calculated on the assumption that the respective parent ions are formed with $v_2^+ = v_2'$). The shapes of the two distributions are similar, though the distribution in Figure 2b extends to higher TKER, implying that at least some of the parent vibrational energy is partitioned into product translational energy. Analysis of the distributions shown in Figure 2 reveals that ~25% of the available energy [E_{avl}, defined by $E_{avl} = h\nu_2 - D_0(H_2N^+-H)$] is partitioned into TKER of the H + NH_2^+ fragments in these cases (cf. a TKER of <5% in the case of the corresponding fragments from dissociative ionization with the REMPI laser alone).

Figure 3 compares the TKER distributions of the H + NH_2^+ fragments resulting from 207.6 nm photolysis of $NH_3^+(\tilde{X})$ cations prepared by 2 + 1 REMPI of NH_3 via the $v_2' = 2$ levels of (a) the $\tilde{C}'$ state and (b) the $\tilde{B}$ state. The two TKER distributions are essentially identical, consistent with expectations that both REMPI schemes favor formation of $v_2^+ = 2$ parent ions. The vertical arrow in Figure 3a indicates the maximum TKER allowed by energy conservation on the basis that dissociation is from $NH_3^+(\tilde{X}, v_2^+ = 2)$ parent ions. These distributions are qualitatively similar to those displayed in Figure 2 but show a further extension to higher TKER, again implying some partitioning of parent vibrational energy into product translation. Again, it is clear that the bulk of E_{avl} (~80% in this case) is partitioned into internal excitation of the NH_2^+ fragment, but the available resolution is insufficient to reveal details of this excitation (e.g. product rotation and/or vibration).

Similar experiments have been performed with the ND_3^+ cation. Figure 4 shows TKER distributions of the D + ND_2^+ fragments resulting from 207.6 nm photolysis of ND_3^+ cations formed by 2 + 1 REMPI of ND_3 at, respectively, $\lambda_1 =$ (a) 303.2 nm ($\tilde{\nu}_1 = 32\,978$ cm^{-1}), (b) 296.8 nm (33 696 cm^{-1}), (c) 306.3 nm (32 648 cm^{-1}) and (d) 295.6 nm (33 826 cm^{-1}), i.e. at REMPI wavelengths that are two photon resonant with Q branch features within, respectively, the $\tilde{C}'-\tilde{X}$ 2_0^3 and 2_0^5 transitions and the $\tilde{B}-\tilde{X}$ 2_0^8 and 2_0^{11} bands. These TKER distributions are qualitatively similar to those of the H + NH_2^+ products displayed in Figures 2 and 3. Each exhibits a fast tail extending to the limit allowed by energy conservation (on the basis that the parent ions are formed with $v_2^+ \sim v_2'$), but the fraction of the available energy partitioned into D + ND_2^+ product translation is consistently lower, declining from ~15% in the case of excitation via the $v_2' = 3$ level to ~12% when exciting via $v_2' = 11$. These energy disposal estimates are derived by

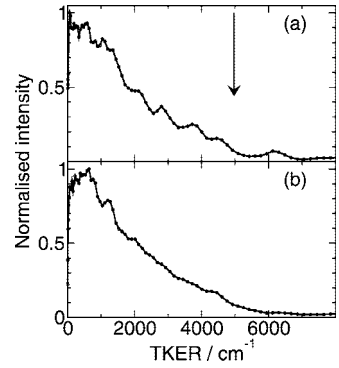

Figure 3. TKER distributions of the H + NH_2^+ fragment ions resulting from 2 + 1 REMPI of NH_3 via the $v_2' = 2$ levels of the (a) $\tilde{C}'$ and (b) $\tilde{B}$ states with subsequent photolysis of the resulting parent cations at $\lambda_2 = 207.6$ nm after $\delta t \sim 20$ ns. The vertical arrow indicates the maximum TKER of the H + $NH_2^+(\tilde{X})$ fragments resulting from one-photon dissociation of parent cations with $v_2^+ = v_2'$.

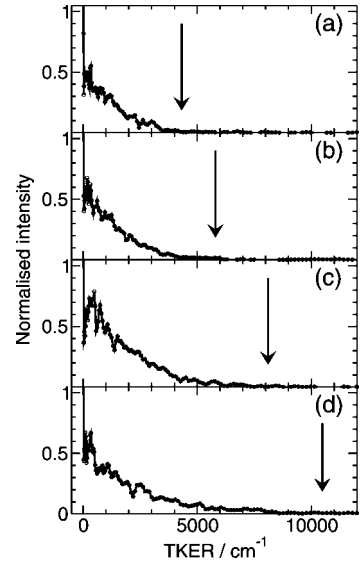

Figure 4. TKER distributions of the D + ND_2^+ products resulting from 2 + 1 REMPI of ND_3 via the following levels: (a) $\tilde{C}'$, $v_2' = 3$; (b) $\tilde{C}'$, $v_2' = 5$; (c) $\tilde{B}$, $v_2' = 8$; and (d) $\tilde{B}$, $v_2' = 11$ with, in each case, subsequent photolysis at $\lambda_2 = 207.6$ nm after $\delta t \sim 20$ ns. The vertical arrow in each panel indicates the maximum speed of $ND_2^+(\tilde{X})$ fragment ions resulting from one-photon dissociation of parent cations with $v_2^+ = v_2'$. The peak at TKER ~ 0 is attributed to unintended ionization of NH_2D molecules (which also appear as ions with m/z 18) present in the molecular beam. The vertical scale in each plot has been chosen so that the D + ND_2^+ TKER distributions of interest are all normalized to the same peak intensity, with the result that the near-zero velocity peak is off-scale.

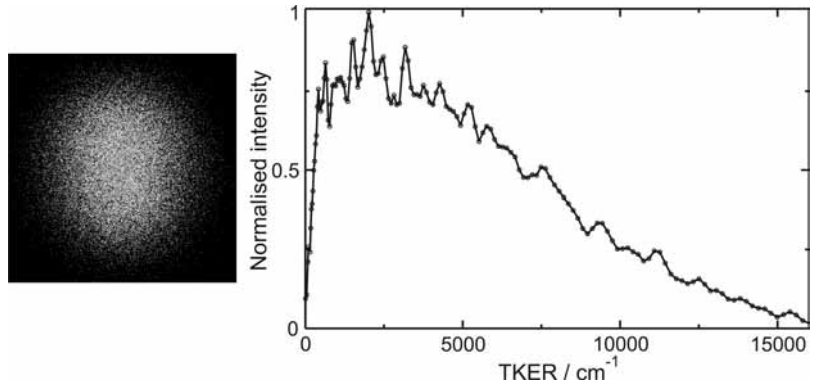

Figure 5. Raw image of the m/z 15 (NH^+) fragments resulting from multiphoton excitation of NH_3 at $\lambda_1 = 283.8$ nm ($\tilde{\nu}_1 = 35\,234$ cm^{-1}), along with the associated product TKER distribution (calculated assuming that the products are $NH^+ + H_2$).

assuming $D_0(D_2N^+-D) = 5.691 \pm 0.001$ eV[37] and that the ionization step in the 2 + 1 REMPI process is Franck−Condon diagonal [i.e., that $\Delta v = (v_2^+ - v_2') = 0$]. We note that the earlier 2 + 1 REMPI-photoelectron studies (of NH_3) revealed a progressive increase in the probability of $\Delta v < 0$ transitions upon ionization from high v_2' levels of the $\tilde{B}$ state.[32] Such behavior, if repeated in ND_3, would cause us to overestimate the effective E_{avl} and thus to underestimate the fractional energy partitioning into ND_2^+ internal excitation, which may explain part (or all) of the apparent decline in the latter reported above. As Figure 4 shows, each of these distributions also exhibits a large peak at zero TKER, which manifests itself as an intense central dot in the measured images. Only parent ions are likely to be formed with zero recoil velocity, and this feature is most readily attributable to unintended 1 + 1 REMPI of a small fraction of NH_2D impurity in the ND_3 sample by 207.6 nm radiation, yielding parent NH_2D^+ ions with m/z 18.

The TKER distributions of the H + NH_2^+ and D + ND_2^+ products measured in the two-color studies all have broadly similar appearance, peaking near zero, and thereby implying that most of the available energy is partitioned into internal excitation of the fragment cation. The overall shapes of these TKER distributions accord well with the earlier statistical phase space predictions.[25] Such a statistical treatment of the product energy disposal would be reasonable, given initial photoexcitation of the $NH_3^+(\tilde{X}, v_2^+)$ cation to the $\tilde{A}^2E$ state, rapid radiationless transfer to high levels of the $\tilde{X}$ state via one, or more, CIs linking the $\tilde{A}$ and $\tilde{X}$ state PESs[15] and subsequent intramolecular vibrational redistribution (IVR) on the ground-state PES en route to eventual N−H bond fission and NH_2^+ product formation.

3.3. One-Color Studies of NH^+ Product formation. As mentioned previously, NH^+ fragment ion signals were increasingly apparent as the REMPI wavelength was reduced. An NH^+ signal was also observed from the photolysis laser alone ($\lambda_2 = 207.6$ nm). No NH^+ signal that was dependent on both the REMPI and photolysis laser pulses could be identified with confidence. Figure 5 shows a raw image of the m/z 15 (NH^+) fragments resulting from multiphoton excitation of NH_3 at a wavelength $\lambda_1 = 283.8$ nm ($\tilde{\nu}_1 = 35\,234$ cm^{-1}), chosen to be two-photon resonant with the $\tilde{C}'$, $v_2' = 7$ level, along with the product TKER distribution derived by assuming the unobserved cofragment to be H_2. This image shows no discernible recoil anisotropy. The TKER distribution shown in Figure 5 peaks at low TKER (~2000 cm^{-1}) but extends to ~16 000 cm^{-1}, implying a propensity for forming products with substantial internal excitation.

The electron-induced dissociative ionization studies[24] suggest a value of 16.9 ± 0.1 eV (measured relative to the ground-state neutral) for the threshold energy for forming $NH^+ + H_2$ products. The photon energy used in recording the image shown in Figure 5 is 4.368 eV. Possible routes to forming NH^+ fragments in the present experiments could thus involve multiphoton absorption and subsequent dissociative ionization, i.e.

$$NH_3(\tilde{X}^1A_1) + nh\nu_1 \rightarrow NH^+ + H_2 + e^- \quad (5)$$

with $n \geq 4$, or multiphoton excitation of NH_3^+ parent ions formed by 2 + 1 REMPI of NH_3, i.e.

$$NH_3^+(\tilde{X}, v_2^+) + mh\nu_1 \rightarrow NH^+ + H_2 \quad (6)$$

with $m \geq 2$. (The low NH_2^+ yields tend to exclude NH_2^+ fragment photolysis as the source of the observed NH^+ products). Energy conservation dictates that the maximum TKER of products arising via process 5 when $n = 4$ is ~4700 ± 800 cm^{-1}. The measured distribution extends to much higher TKER and shows no obvious discontinuity at TKER ~ 4700 cm^{-1}. Thus, we conclude that $n \geq 5$ would be required if the observed NH^+ fragments arise via multiphoton absorption and subsequent dissociative ionization (process 5). The maximum possible TKER in the case where $n = 5$ (~40 000 cm^{-1}) is far in excess of that observed, but the measured distributions could be understood if the NH^+ fragments were formed electronically excited (e.g. in the $A^2\Sigma^-$ or $B^2\Delta$ excited states) and/or the NH^+ and H_2 products were formed internally (vibrationally and rotationally) excited.

We now consider the alternative route (process 6). As in the one-color studies of NH_2^+ fragment ion formation (section 3.1), one-photon excitation of the parent cation (i.e., $m = 1$ in eq 6) provides insufficient energy to reach the reported threshold for NH^+ production, but two-photon excitation of $NH_3^+(\tilde{X}, v_2^+ = 7)$ cations could yield $NH^+ + H_2$ fragments with TKER ≤ 23 000 ± 800 cm^{-1}. Again, the measured images could be accommodated if one, the other, or both of these fragments were formed with substantial internal (vibrational and rotational) excitation. As in the case of the NH_2^+ products, such energy disposal and the isotropic nature of the NH^+ product recoil velocity distribution both hint at a dissociation mechanism that involves coupling to high levels of the ground state, IVR and statistical distribution of population among the various product modes.

The early ab initio calculations of Rossi and Avouris[21] suggest a possible explanation for the present observations. These calculations found global minima for the $^2A'$ and $^2A''$ components of the JT distorted $\tilde{A}^2E$ state, and showed that the latter was characterized by two long N−H bonds and a short H···H distance, a structure appropriate for eventual dissociation by

H_2 elimination. This study anticipates fragmentation behavior that broadly parallels the present observations. Vertical excitation (from the $\tilde{X}^2A_2''$ state in the present study) with progressively more energetic photons would first sample the $^2A'$ component of the $\tilde{A}$ state, which dissociates by rapid radiationless transfer to the ground-state and subsequent unimolecular decay to $H + NH_2^+$ fragments. Excitation at higher energies (achieved using two photons in the present study) is predicted to populate the $^2A''$ component also and to result in some eventual fragmentation (either diabatically or following transfer to the ground state) by H_2 elimination.

Conclusions

The present analyses of velocity map images of NH_2^+, (ND_2^+), and NH^+ fragment ion images resulting from photolysis of state selected NH_3^+ (and ND_3^+) cations serve to reinforce and extend previous discussions of the photofragmentation dynamics of the ammonia cation.

The two-color measurements use 2 + 1 REMPI via selected levels of the $\tilde{B}$ and $\tilde{C}'$ states to prepare vibrationally (υ_2^+) state-selected parent cations, which are then photolyzed (at 207.6 nm) by absorption from a second laser pulse. The TKER distributions of the resulting $H + NH_2^+$ ($D + ND_2^+$) fragments are isotropic, peak at low KEs, but extend to the highest TKERs allowed by energy conservation. Such findings accord with results obtained in earlier electron-induced photoionization[24] and PEPICO[25] studies of NH_3 at similar total energies (defined relative to the ground-state neutral) and can be rationalized in terms of excitation to (the $^2A'$ component of) the Jahn−Teller distorted $\tilde{A}^2E$ state, rapid radiationless transfer via one or more CIs linking the $\tilde{A}$ and $\tilde{X}$ state PESs, and subsequent unimolecular decay to $H + NH_2^+$ fragments on the ground-state PES.[15]

Weak NH_2^+ and NH^+ fragment ion signals are also observed in experiments that employ the REMPI laser only. The TKER distributions of these fragments are also isotropic and peak at low KEs. One-photon excitation at the REMPI laser wavelengths used in this study provides insufficient energy to excite $NH_3^+(\tilde{X}, \upsilon_2^+)$ cations above the threshold for N−H bond fission or the deduced energetic onset for elimination of H_2 products. The measured one-color NH_2^+ fragment images are most readily interpreted by assuming four-photon excitation and subsequent dissociative ionization of some fraction of the neutral NH_3 sample. The measured NH^+ fragment images might be attributable to a similar multi- (five-) photon excitation followed by dissociative ionization pathway, but the observed distributions could alternatively be accommodated in terms of two-photon excitation of $NH_3^+(\tilde{X}, \upsilon_2^+)$ cations (themselves formed by 2 + 1 REMPI) to the $^2A''$ JT component of the $\tilde{A}^2E$ state with subsequent radiationless transfer to the ground-state and unimolecular elimination of H_2.

Acknowledgment. Financial support from the EPSRC (Portfolio Partnership award LASER) is gratefully acknowledged, as is the help and advice provided by Bristol colleagues Prof. R. N. Dixon, Dr. C. M. Western, and K. N. Rosser.

References and Notes

(1) Ashfold, M. N. R.; Nahler, N. H.; Orr-Ewing, A. J.; Vieuxmaire, O. P. J.; Toomes, R. L.; Kitsopoulos, T. N.; Anton-Garcia, I.; Chestakov, D.; Wu, S.-M.; Parker, D. H. *Phys. Chem. Chem. Phys.* **2006**, *8*, 26.

(2) Webb, A. D.; Nahler, N. H.; Dixon, R. N.; Ashfold, M. N. R. *J. Chem. Phys.* **2006**, *125*, 204312.

(3) Vieuxmaire, O. P. J.; Nix, M. G. D.; Fitzpatrick, J. A. J.; Beckert, M.; Dixon, R. N.; Ashfold, M. N. R. *Phys. Chem. Chem. Phys.* **2004**, *6*, 543.

(4) Nahler, N. H.; Vieuxmaire, O. P. J.; Jones, J. R.; Ashfold, M. N. R.; Eppink, A.T.J.B.; Coriou, A. M.; Parker, D. H. *J. Phys. Chem. A.* **2004**, *108*, 8077.

(5) Vieuxmaire, O.P.J., N.H.; Nahler, N.H., J.R.; Jones, J. R.; Dixon, R. N.; Ashfold, M. N. R. *Mol. Phys.* **2005**, *103*, 2437.

(6) Vieuxmaire, O. P. J.; Nahler, N. H.; Dixon, R. N.; Ashfold, M. N. R. *Phys. Chem. Chem. Phys.* **2007**, *9*, 5531.

(7) Chang, C. S.; Luo, C. Y.; Liu, K. P. *J. Phys. Chem. A.* **2005**, *109*, 1022.

(8) Webb, A. D.; Dixon, R. N.; Ashfold, M. N. R. *J. Chem. Phys.* **2007**, *127*, 224307.

(9) Webb, A. D.; Kawanaka, N.; Dixon, R. N.; Ashfold, M. N. R. *J. Chem. Phys.* **2007**, *127*, 224308.

(10) Kim, M. H.; Leskiw, B. D.; Suits, A. G. *J. Phys. Chem. A.* **2005**, *109*, 7839.

(11) Kim, M. H.; Leskiw, B. D.; Shen, L.; Suits, A. G. *J. Phys. Chem. A.* **2007**, *111*, 7472.

(12) Lee, S. K.; Silva, R.; Kim, M. H.; Shen, L.; Suits, A. G. *J. Phys. Chem. A.* **2007**, *111*, 6741.

(13) Rabalais, J. W.; Karlsson, L.; Werme, L. O.; Bergmark, T.; Siegbahn, K. *J. Chem. Phys.* **1973**, *58*, 3370.

(14) Edvardsson, D.; Baltzer, P.; Karlsson, L.; Wannberg, B.; Holland, D. M. P.; Shaw, D.; Rennie, E. E. *J. Phys. B.* **1999**, *32*, 2583.

(15) Woywod, C.; Scharfe, S.; Krawczyk, R.; Domcke, W.; Köppel, H. *J. Chem. Phys.* **2003**, *118*, 5880.

(16) Bawendi, M. G.; Rehfuss, B. D.; Dinelli, B. M.; Okomura, M.; Oka, T. *J. Chem. Phys.* **1989**, *90*, 5910.

(17) Lee, S. S.; Oka, T. *J. Chem. Phys.* **1991**, *94*, 1698.

(18) Dujardin, G.; Leach, S. *Can. J. Chem.* **1985**, *63*, 1386.

(19) Köppel, H.; Cederbaum, L. S.; Domcke, W.; von Niessen, W. *Mol. Phys.* **1978**, *35*, 1283.

(20) Haller, E.; Cederbaum, L. S.; Domcke, W.; Köppel, H. *Chem. Phys. Lett.* **1980**, *72*, 427.

(21) Rossi, A. R.; Avouris, P. *J. Chem. Phys.* **1983**, *79*, 3413.

(22) Krier, C.; Praet, M. Th.; Lorquet, J. C. *J. Chem. Phys.* **1985**, *82*, 4073.

(23) Viel, A.; Eisfeld, W.; Neumann, S.; Domcke, W.; Manthe, U. *J. Chem. Phys.* **2006**, *124*, 214306.

(24) Locht, R.; Servais, Ch.; Ligot, M.; Derwa, F. R.; Momigny, *J. Chem. Phys.* **1988**, *123*, 443.

(25) Powis, I. *J. Chem. Soc. Faraday Trans.* **1981**, *77*, 1433.

(26) Song, Y.; Qian, X.-M.; Lau, K.-C.; Ng, C. Y.; Liu, J.; Chen, W. *J. Chem. Phys.* **2001**, *115*, 2582.

(27) Habernicht, W.; Reiser, G.; Müller-Dethlefs, K. *J. Chem. Phys.* **1993**, *98*, 8462.

(28) Willitsch, S.; Merkt, F.; Kallay, M.; Gauss, J. *Mol. Phys.* **2006**, *104*, 1457.

(29) Mordaunt, D. H.; Ashfold, M. N. R.; Dixon, R. N. *J. Chem. Phys.* **1996**, *104*, 6460.

(30) Langford, S. R.; Orr-Ewing, A. J.; Morgan, R. A.; Western, C. M.; Ashfold, M. N. R.; Rijkenberg, A.; Scheper, C. R.; Buma, W. J.; de Lange, C. A. *J. Chem. Phys.* **1998**, *108*, 6667, and references therein.

(31) Glownia, J. H.; Riley, S. J.; Colson, S. D.; Miller, J. C.; Compton, R. N. *J. Chem. Phys.* **1982**, *77*, 68.

(32) Conaway, W. E.; Morrison, R. J. S.; Zare, R. N. *Chem. Phys. Lett.* **1985**, *113*, 429.

(33) Eppink, A.T.J.B.; Parker, D. H. *Rev. Sci. Instrum.* **1997**, *68*, 3477.

(34) Wrede, E.; Laubach, S.; Schulenburg, S.; Brown, A.; Wouters, E. R.; Orr-Ewing, A. J.; Ashfold, M. N. R. *J. Chem. Phys.* **2001**, *114*, 2629.

(35) Wood, R. W. *Philos. Mag.* **1902**, *4*, 396.

(36) Ashfold, M. N. R.; Bennett, C. L.; Dixon, R. N. *Chem. Phys.* **1985**, *93*, 293.

(37) Qian, X.-M.; Lau, K.-C.; He, G. Z.; Ng, C. Y.; Hochlaf, M. *J. Chem. Phys.* **2004**, *120*, 8476.

JP808854D